# Effect of an Interactive Surface on the Equilibrium Contact Angles in Bilayer Polymer Films

D. Slep,[†,‡] J. Asselta,[‡] M. H. Rafailovich,*[,‡] J. Sokolov,*[,‡] D. A. Winesett,[§] A. P. Smith,[§] H. Ade,[§] and Simone Anders[||]

*Hilord Chemical Corporation, Hauppauge, New York 11788, Department of Material Science, State University of New York at Stony Brook, Stony Brook, New York 11974-2275, Department of Physics, North Carolina State University, Raleigh, North Carolina 27596, and Advanced Light Source, Ernest Orlando Lawrence Berkeley National Laboratory, University of California, Berkeley, California 94720*

*Received January 12, 1999. In Final Form: November 2, 1999*

Scanning transmission X-ray microscopy (STXM), atomic force microscopy (AFM), near-edge X-ray absorption fine structure (NEXAFS) spectroscopy, and photoemission electron microscopy (PEEM) were used to obtain the three-dimensional concentration profiles and the late-stage morphology of liquid bilayer thin films of the two imiscible polymers polystyrene (PS) and (polybromostyrene) ($PBr_{x=0.79}S$), where $x$ = fraction of monomers brominated) as a function of the lower PS film thickness. The results showed that the apparent contact angle at the polymer/air interface decreases exponentially with increasing PS film thickness with a constant that scales with the PS radius of gyration ($R_g$). In contrast, the Neuman angle, as determined from the PBrS STXM images, increases with substrate thickness. NEXAFS and PEEM data show that the droplets consist of a PBrS core fully encapsulated by PS for substrate thicknesses greater than $R_g$. Only partial encapsulation is seen for substrates less than $R_g$. These results could not be explained with existing models developed for bulk viscoelastic fluids. We found that, for the case of entangled polymers, other factors such as the interfacial energy with the substrate, the film thickness, and the molecular weights must be considered. A model which includes a restoring force characterizing the change in stiffness of the substrate layer due to surface interactions provided good agreement with the experimental observations.

## Introduction

Thin film polymer blends have numerous technological applications in diverse areas such as color photographic printing to paints, adhesives, and protective coatings. Consequently, there has been intense activity in recent years in trying to understand the dewetting mechanisms involved from solid and liquid substrates.[1,2] In particular, much effort has been concentrated on combining classical theories of simple liquids with mean field theories to predict miscibility parameters in polymer blends. For example the well-known Flory−Huggins parameter, $\chi$, which determines miscibility, has been shown to relate to the interfacial forces within mean field theory in the following equation:[3]

$$\gamma_{A/B} = a\rho k_B T(\chi/6)^{1/2} \quad (1)$$

where $1/\rho$ is the monomer volume and $\gamma_{A/B}$ is the interfacial force. Measurements of $\chi$ using the standard techniques of small-angle neutron or X-ray scattering can be very tedious and often not practical when $\chi$ is very large.[4] Measuring the contact angle between polymers in bilayer thin films has recently been proposed as an alternative.[5,6] The interfacial tension between a liquid droplet and a solid substrate can be obtained from the classical Young's relationship:

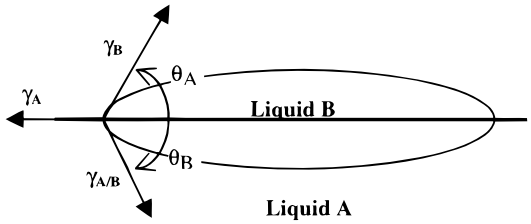


**Figure 1.** A−B Liquid−liquid interface balancing of interfacial and surface forces produce $\theta_A$, the angle that can be measured by the topography, and $\theta_B$, the Neuman angle.

$$\gamma_A - (\gamma_{A/B} + \gamma_B \cos\theta) = 0 \quad (2)$$

where $\gamma_A$ and $\gamma_B$ are the surface energies of two polymers and $\theta$ is the angle formed on a rigid surface by a fluid droplet at equilibrium conditions. In the case of liquid bilayers that undergo lamellar phase separation, the effective contact angle is no longer constrained to the interface and the Neuman angle must now be considered[2] Figure 1). From Figure 1, we see that in a liquid/liquid system the effective contact angle, which is the angle that can be measured by the topography, is given by

$$\theta_E = \theta_A + \theta_B \quad (3)$$

where $\theta_A$ and $\theta_B$ are the topographical apparent angle formed by liquid A and the Neuman angle, which extends below the liquid/liquid interface. Balancing of interfacial

[†] Hilord Chemical Corp.
[‡] State University of New York at Stony Brook.
[§] North Carolina State University.
[||] University of California.

(1) Qu, S.; Clarke, C. J.; Liu, Y.; Rafailovich, M. H.; Sokolov, J.; Phelan, K. C. Krausch, G. *Macromolecules* **1997**, *30*, 3640.
(2) Wyart, F. B.; Martin, P.; Redon, C. *Langmuir* **1993**, *9*, 3682.
(3) Helfand, E.; Tagami, Y. Polym. Lett. **1971**, *9*, 741; *J. Chem. Phys.* **1971**, *56*, 3592.
(4) Clarke, C. J.; Eisenberg, A.; La Scala, J.; Rafailovich, M. H.; Sokolov, J.; Li, Z.; Qu, S.; Nguyen, D.; Schwartz, S. A.; Strzhemechny, Y.; Sauer, B. B. *Macromolecules* **1997**, *30*, 4184.
(5) Vitt, E.; Schull, K. R. *Macromolecules* **1995**, *28*, 6349.
(6) Israels, R.; Jasnow, D.; Balazs, A. C.; Guo, L.; Krausch, G.; Sokolov, J.; Rafailovich, M. *J. Chem. Phys.* **1995**, *102*, 8149.

10.1021/la990031b CCC: $19.00 © 2000 American Chemical Society
Published on Web 01/11/2000

and surface forces gives the other two classical Neuman equations:

$$\gamma_A = \gamma_B \cos \theta_A + \gamma_{A/B} \cos \theta_B \quad (4)$$

$$\gamma_{A/B} \sin \theta_B = \gamma_B \sin \theta_A \quad (5)$$

In thin film polymer systems, the effective contact angle of two immiscible liquids becomes more complex because of the influences of polymer entanglements and the interfacial forces of the substrate with the two polymers. We will show that the topographical information is insufficient to obtain a quantitative result. Rather it is important to determine the three-dimensional concentration profiles of the components and consider the effects of the substrate interactions on the conformation of the polymer chains.

In this paper, we concentrated on the late-stage morphology of liquid bilayer thin films of the two imiscible polymers, polystyrene (PS) and poly(bromostyrene) of degree of bromination $x = 0.79$ ($PBr_{x=0.79}S$). Both PS and PBrS wet the silicon surface, but dewet each other. The surface morphology and the microscopic contact angles were imaged with an atomic force microscope (AFM). Since the frictional and mechanical properties of PS and PBrS are similar, scanning force microscopies could not be used to distinguish between the two components.[7] Because of the complex nature of the system described, we took advantage of scanning transmission X-ray microscopy (STXM), which could discern lateral chemical differences with a spatial resolution of 400 Å. The data from the STXM was also used to calculate the complete Newman angle, which was compared to the Young's contact angle as determined from the surface topography. The relationship between the two quantities is fairly straightforward for simple liquids. In Results and Discussion, we will show that, in the case of polymers, other factors such as the interfacial energy with the substrate, the film thickness, and the molecular weights must be considered.

## 2. Experiment

Monodisperse ($M_w/M_n \cong 1.0$) PS of molecular weights 96K and 575K from Polymer Laboratory were used in these experiments. The $PBr_{x=0.79}S$ samples were made from the 96K MW batch of PS by the bromination procedure described by Kambour et al.[8] The bromine is on the c4 position in the aromatic ring, making the compound poly(*p*-bromostyrene). The same batch of polystyrene was used for all samples that were brominated, in the thin films and in the samples for bulk analysis.

The bulk polystyrene and poly(bromostyrene) samples were characterized with mass analysis and differential scanning calorimetry (DSC). Bulk samples from the same batch used for the films were sent to Dessert Analytical for a mass analysis of bromine content in $PBr_xS$ and were found to have a degree of bromonation of approximately 79% ($PBr_{x=0.79}S$).

The glass transition temperatures ($T_g$) were measured on PS and $PBr_{x=0.79}S$ using a Mettler T11 DSC, and the results were very close to published values.[9]

| sample | accepted $T_g$ values, °C | measd $T_g$ |
|---|---|---|
| PS standard 96K | 109 | 109.5 |
| $PBr_{x=0.79}S$ | 142 (for $x = 1$) | 139.1 |

To remove the oxide layer, the silicon wafer substrates were first cleaned by heating above 80 °C in a solution of deionized water, hydrogen peroxide, and ammonium. The silicon wafers were then dipped in a water and hydrofluoric acid solution, until a hydrophobic surface was obtained.[10] The films were spun cast immediately after this step in order to reduce the amount of oxidation of the substrate. Bilayer samples prepared in native oxide covered Si wafers would occasionally dewet the substrate and produced inconsistent results.

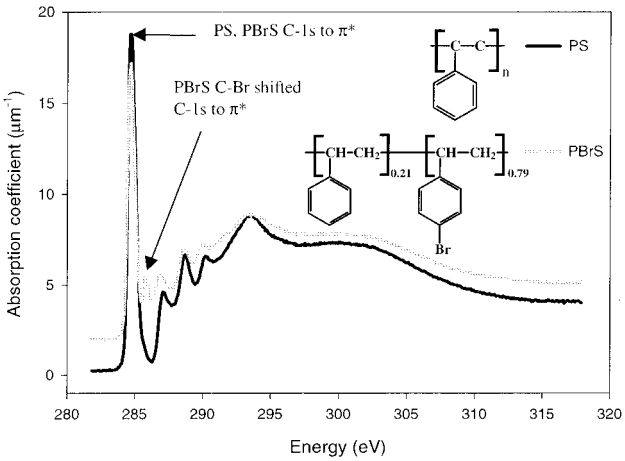


**Figure 2.** NEXAFS reference spectra of PS and PBrS normalized to the Henke pre- and post edge absorption coefficients.

Solutions were made of monodisperse PS ($M_w = 96K$ and 575K, $M_w/M_n \cong 1.0$) and $PBr_{x=0.79}S$ dissolved in chlorobenzene, at different solid-to-solvent ratios in order to control film thickness. The samples were prepared by spin casting the PS layer first on the HF etched Si substrates. The $PBr_{x=0.79}S$ layer was then floated on top from a deionized water surface. A number of different samples were made with different thicknesses of the PS layer of both molecular weights. Note that the solutions were allowed to sit overnight before being spun cast onto the silicon in order to achieve complete dissolution of the two polymers. Films were spun at a rate of 2500 revolutions per minute (rpm) for 60 s. The thicknesses of the films were measured with a Rudolph 3 wavelength model "auto EL" ellipsometer.

The films were annealed at 180 °C in a vacuum of $10^{-4}$ Torr for times varying from 2 h to 21 days until very little change in the surface morphology was observed. The samples were then quenched in atmospheric pressure air to room temperature. In other words, the samples were annealed to equilibrium in a liquid state and then rapidly quenched to the solid state. The topography of the samples was analyzed with a DI 3000 atomic force microscope (AFM) in the contact mode using a $Si_3N_4$ tip.

A small corner of the samples was floated from the silicon substrates onto carbon coated grids by dipping in KOH solution at 80° C which attacks the native oxide layer. The samples were subsequently studied with scanning transmission X-ray microscopy on beamline X1A (X1A-STXM) at the National Synchrotron Light Source at Brookhaven National Laboratory. The X1A-STXM utilizes zone plate optics to produce a microprobe, whose size of about 50 nm determines the spatial resolution. The samples are imaged in transmission mode in an atmospheric pressure He enclosure. Details about the instrument are described by Jacobsen et al.[11]

To be able to perform quantitative compositional mapping, near-edge X-ray absorption fine structure spectroscopy (NEXAFS) reference spectra were acquired of PS and $PBr_{x=0.79}S$ thin films with STXM (Figure 2). The pre-carbon-edge (280 eV) and post-carbon-edge atomic continuum (317 eV) values from these spectra were scaled to the atomic X-ray absorption coefficients from the database of Henke et al.,[12] assuming a uniform density of 1.07 g/cm$^3$ for PS and 1.53 g/cm$^3$ for $PBr_{x=0.79}S$.[9]

(7) Krausch, G.; Hipp, M.; Boltau, M.; Marti, O.; Mlynek, J. *Macromolecules* **1995**, *28*, 260.
(8) Kambour, R. P.; Bendler J. T.; Bopp R. C. *Macromolecules* **1983**, *16*, 753.
(9) Bicerano, J. *Predict. Polym. Prop.* **1993**, 154.
(10) Higashi, G. S.; Chabal, Y. J.; Trucks G. W.; Raghavachari K. *Appl. Phys. Lett.* **1990**, *56*, 656.
(11) Jacobsen, C.; Williams, S.; Anderson, E.; Brown, M. T.; Buckley, C. J.; Kern, D.; Kirz, J.; Rivers, M.; Zhang, X. *Opt. Commun.* **1991**, *86*, 351.
(12) Henke, B. L.; Gullikson, E. M.; Davis, J. C. *At. Data Nucl. Data Tables* **1993**, *54*, 2, 181.

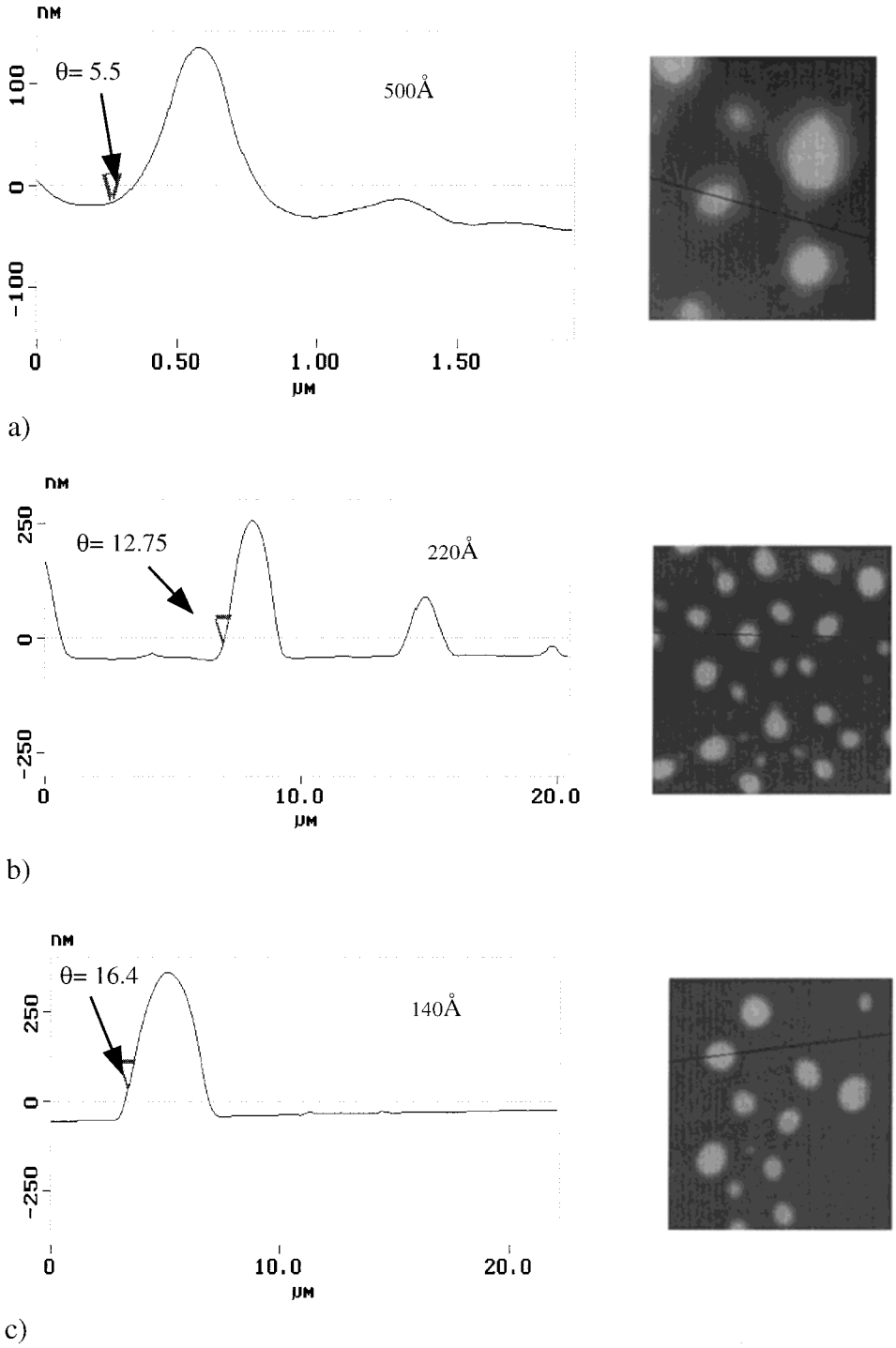


**Figure 3.** AFM image of a PS/PBrS annealed bilayer film with a PS sublayer of (a) 500 Å (2 $\mu$m by 2 $\mu$m image), (b) 220 Å (20 $\mu$m by 20 $\mu$m image) and (c) 140 Å (25 $\mu$m by 25 $\mu$m image) where the light areas are raised.

Utilizing these normalized absorption coefficients and several characteristic X-ray micrographs of the sample under investigation, we can extract quantitative equivalent thickness maps for the two components with a spatial resolution of 50 nm by employing a singular value decomposition procedure.[13]

### 3. Results and Discussion

Parts a−c of Figure 3 show the AFM images of a series of samples which were initially bilayers of $PBr_{x=0.79}S$ ($M_w$ = 96K, thickness ≅ 300 Å) and PS ($M_w$ = 96K; thickness = 500, 220, and 140 Å), where the PS layer was spun cast directly onto the HF etched Si substrate. The samples were annealed at 180 °C for times ranging from 2 h to 2 weeks. Further annealing did not change the morphology, and hence the figures shown were assumed to be the equilibrium configurations. Since PS and PBrS have glass transitions above room temperature and similar chemical structures, negligible mechanical and frictional differences exist between the two materials. Consequently, only topographical images could be obtained. From the AFM images, it is possible to extract what appears to be the contact angle between the layer adhering to the substrate and the dewetted layer. From Figure 3a−c, it can be seen that the apparent contact angle increases

(13) Zheng, X. Ph.D. Thesis at SUNY Stony Brook, Stony Brook, NY, 1995.

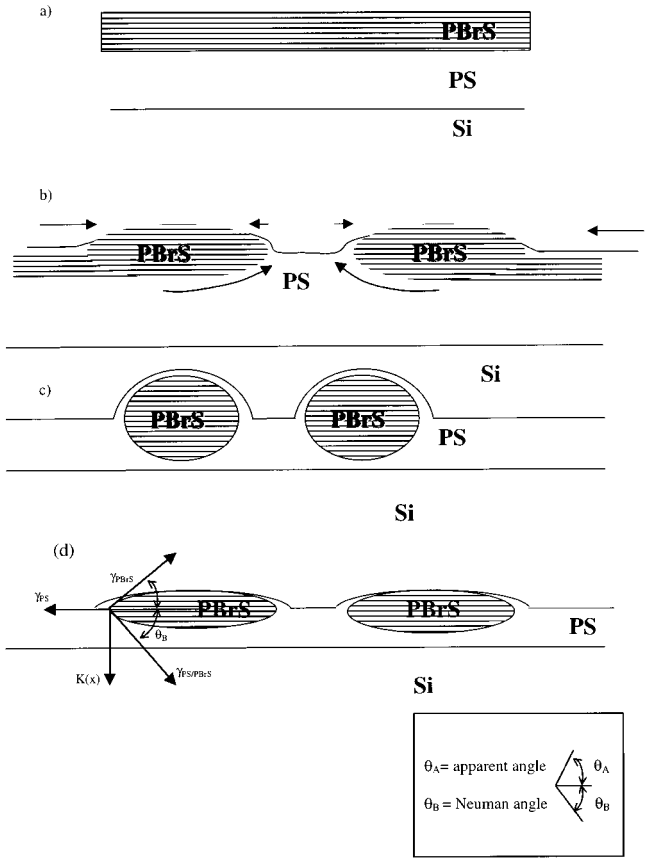


**Figure 4.** Dewetting process of bilayer film (a) as plug flow occurs where the dynamics are dominated by the lower viscosity of the substrate layer holes grow as substrate flows back around the rims (b). Eventually the rims of adjacent holes overlap forming droplet (c) for a thicker film and (d) for a thinner film were encapsulation does not occur. Restoring force $K(x)$ where counterbalances the normal component of the surface tension is shown in (d).

**Table 1**

| | thickness (Å) | mean angle (deg) |
|---|---|---|
| 96 K | 53 | 18.5(1.4) |
| | 111 | 16(0.6) |
| | 140 | 16(1) |
| | 150 | 15(1) |
| | 220 | 12(0.7) |
| | 288 | 8(0.6) |
| | 334 | 6(0.4) |
| | 500 | 4(0.5) |
| | 917 | 3(0.3) |
| 575 K | 104 | 26(3) |
| | 225 | 19(1.6) |
| | 418 | 18(1.4) |
| | 593 | 9(2) |
| | 1166 | 4(1) |

with decreasing PS layer thickness. The thickness values for each PS layer are tabulated in Table 1, together with a similar set of data for PS layer of molecular weight $M_w$ = 575K.

The classical model of the liquid/liquid dewetting[1,2] process is summarized in Figure 4. Holes are produced by strains, such as capillary waves or nucleated holes, in the thin upper layer exposing the lower layer surface. The spreading coefficient, which is proportional to the free energy of the system, is[14]

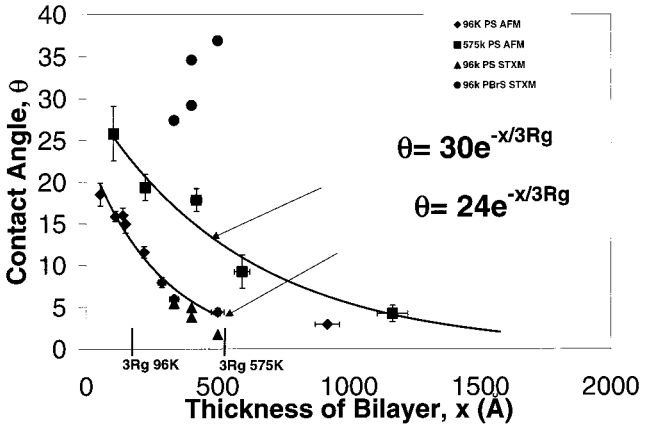


**Figure 5.** $\theta$a from Table 1 as a function of the thickness of the lower PS layer. The solid lines are fits to an exponential decay of the contact angle with film thickness. The decay constant is approximately $3Rg$ for the MW = 96K and MW = 575K polymers.

$$S = \gamma_{PBrS} - (\gamma_{PS} - \gamma_{PS/PBrS}) \tag{6}$$

where $\gamma_{PBrS/PS}$, $\gamma_{PS}$, and $\gamma_{PBrS}$ are the interfacial tension and surface tensions of PS and PBrS, respectively. If $S$ is positive, then the total energy is minimized by exposing the lower layer whose surface energy is lower. If the viscosity of the lower layer is less than the upper layer, the holes grow, as shown in Figure 4, where plug flow occurs as the substrate flows back around the rims. Eventually the rims of adjacent holes overlap, forming a droplet as shown. The equilibrium structure of the droplets is described by the Neuman equations (eq 3−5), where eqs 4 and 5 are rewritten for this system:

$$\gamma_{PS} = \gamma_{PBrS} \cos \theta_A + \gamma_{PS/PBrS} \cos \theta_B \tag{7}$$

$$\gamma_{PS/PBrS} \sin \theta_B = \gamma_{PBrS} \sin \theta_A \tag{8}$$

The decrease in total energy obtained by minimizing the interfacial area between the two polymers, $\gamma_{PS/PBrS}$, is balanced by an energy increase from the increased total surface area given by $\gamma_{PS}$. Since $\gamma_{PS}$ is usually much larger than $\gamma_{PS/PBrS}$ at equilibrium, the area of the droplets below the air surface tends to be larger. To compare our results with the predictions of the "classical model", we can substitute the values for the surface tensions, $\gamma_{ps}$ = 30.5, $\gamma_{PBrS}$ = 33.7, and $\gamma_{PS/PBrS}$ = 1 dyn/cm [15] into eqs 3, 7, and 8. It is apparent that, for these values, $\cos \theta_B > 1$, and we find the Neuman equations are not solvable for the measured contact angles. We therefore must consider that the equations are incomplete for this type of system.

Figure 5 is a plot is of the values of $\theta_A$ versus the thickness of the PS layer from Table 1 for the PS systems of $M_w$ = 96K and 575K. The solid lines are fits to an exponential decay of the contact angle with film thickness. From the figure we see that the initial decay constant is approximately $3R_g$ for the $M_w$ = 96K and $M_w$ = 575K polymers. In contrast to a solid substrate, a polymer substrate is viscoelastic and hence deformable. Consequently we can introduce restoring force $K(x)$ which counterbalances the normal component of the surface tension (Figure 4d). Since the mechanical properties of the polymer substrate are affected by interactions with the solid substrate, the elasticity of the layer and hence

(14) Hobbs, S. Y.; Dekkers, M. E. J.; Watkins, V. H. *Polymer* **1988**, *29*, 1598.

(15) Zhao, W.; Zhao, X.; Rafailovich, M. H.; Sokolov, J.; Mansfield, T.; Stien, R. S.; Composto, R. C.; Kramer, E. J.; Jones, R. A. L.; Sansone, M.; Nelson, M. *Physica B* **1991**, *173*, 43.

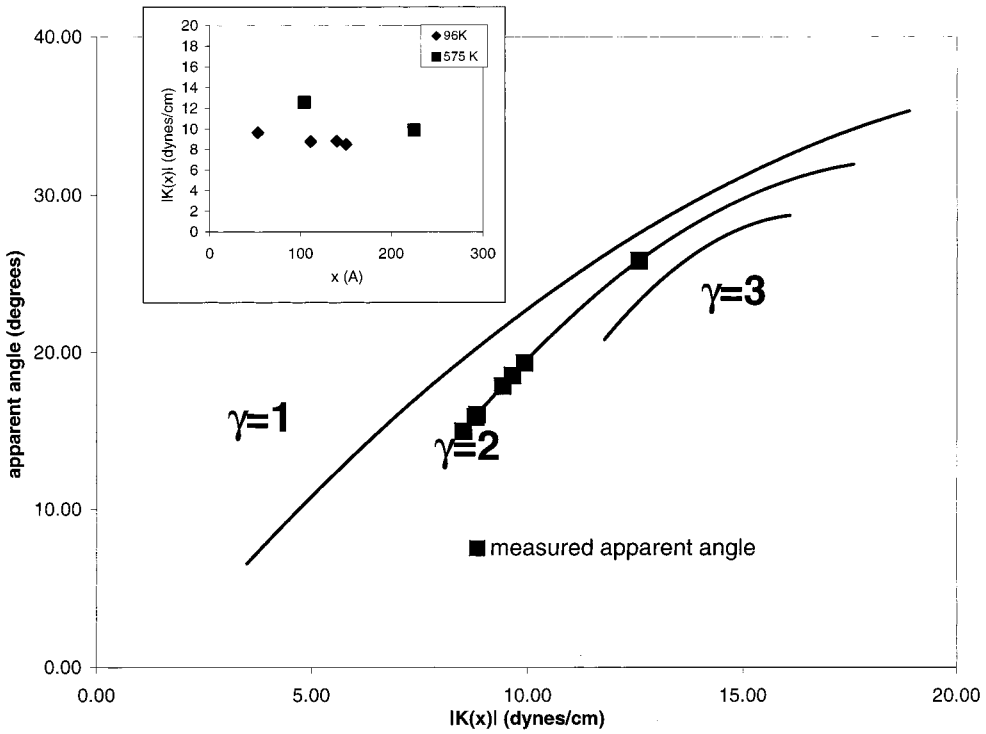


**Figure 6.** Plots of $\theta_a$ versus $K(x)$ for several reasonable values of $\gamma_{PS/PBrS}$.

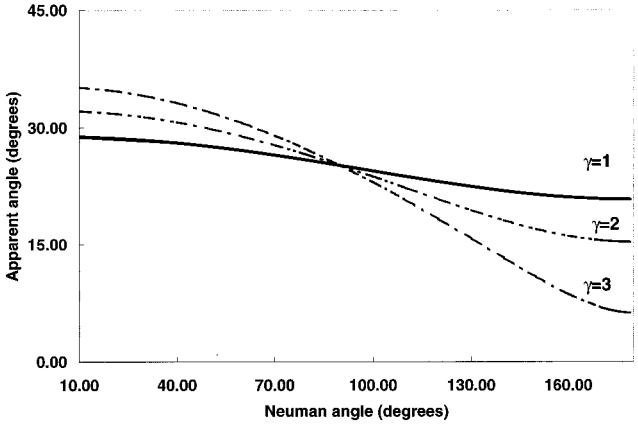


**Figure 7.** Plots of $\theta_a$ versus $\theta_b$ for $\gamma_{PS/PBrS}$ of 1, 2, 3, 4, 5, and 10 dynes/cm.

the restoring force can be thickness dependent. Adding this term to the Neuman eq 8, we obtain

$$\gamma_{PS/PBrS} \sin \theta_B = \gamma_{PBrS} \sin \theta_A - K(x) \qquad (9)$$

Figure 6 shows a plot of $\theta_A$ versus $K(x)$ for three values of $\gamma_{PS/PBrS}$. Using the empirical relationship between $\theta_A$ and film thickness, $x$, from the data in Figure 5, we can now plot $K(x)$ versus $x$ for a reasonable value of $\gamma_{PS/PBrS} =$ 2 dyn/cm. The square shaped points in Figure 6 correspond to the values of $\theta_A$, the apparent contact angle as measured with the AFM. From the figure we can see $K(x)$ is an order of magnitude larger than $\gamma_{PS/PBrS}$ and hence is the determining parameter in the shape of the droplet. Figure 7 shows a plot of $\theta_A$ versus $\theta_B$ for several physically reasonable values of $\gamma_{PS/PBrS}$. From the figure we can see that, at a Neuman angle of approximately 100°, all the traces intersect and, hence, the apparent angle is not sensitive to the interfacial tension.

It has previously been shown[16−20] that the dynamical properties of a polymer melt near an attractive interface can be explained qualitatively by a two fluid model. The fluid layer adjacent to the interface is composed of chains that are pinned to the surface by one or more contacts. Center of mass flow is therefore not possible in this layer, and the mechanical response of this layer should be similar to that of a solid or gel. The rest of the film, defined as the chains that do not have physical contact with the surface, are partially entangled within the first layer. Consequently, an interfacial regime can exist where flow is possible but the dynamics are more sluggish than the bulk.[21] Finally far away from the surface, a factor of 3 radius of gyration or greater, bulk dynamics is restored. It has recently been shown that the rheological response of a liquid polymer film to a scanning probe microscope tip plowing across its surface changed from viscous to solidlike, as the film became thinner. This change in rheological response is also expected to affect the dynamics of dewetting as well as the equilibrium structures and contact angles of the final droplets. Plug flow leading to the structures shown in Figure 4c is only possible in the thick film regime where the response of the substrate is liquidlike. For film thicknesses where flow is not possible, the dewetting behavior of the upper layer is similar to that of the layer on a solid substrate. Consequently, if the structures are PBrS sitting on top of PS, the maximum contact angle could be calculated from Young's equation (eq 2). The calculated value $\theta_A \sim 28.9°$ is still significantly larger than the measured value, $\theta_A = 18.5°$, obtained for a PS layer 53 Å thick. This is due to the fact that even when the substrate is very thin (approximately $R_g$), it can still respond to the normal component of the surface tension at the contact line of the droplet (Figure 4d). We

(16) Karim, A.; Slawecki, T. M.; Kumar, S. K.; Douglas, J. F.; Satija, S. K.; Han C. C.; Russell, T. P.; Liu, Y.; Overney R.; Rafailovich, M. H.; Sokolov, J. *Macromolecules* **1993**, *31*, 857.
(17) Silberzan, P.; Leger, L. *Phys. Rev. Lett.* **1991**, *66*, 185.
(18) Bruinsma, R. *Macromolecules* **1990**, *23*, 276.
(19) Alsten, J. V.; Granick, S. *Macromolecules* **1990**, *23*, 4856.
(20) Hu, H.; Granick, S. *Science* **1992**, *258*, 1339.
(21) Zheng, X.; Rafailovich, M. H.; Sokolov, J.; Strzhemechny, Y.; Schwartz, S. A.; Sauer, B. B.; Rubinstien, M. *Phys. Rev. Lett.* **1997**, *79*, 241.

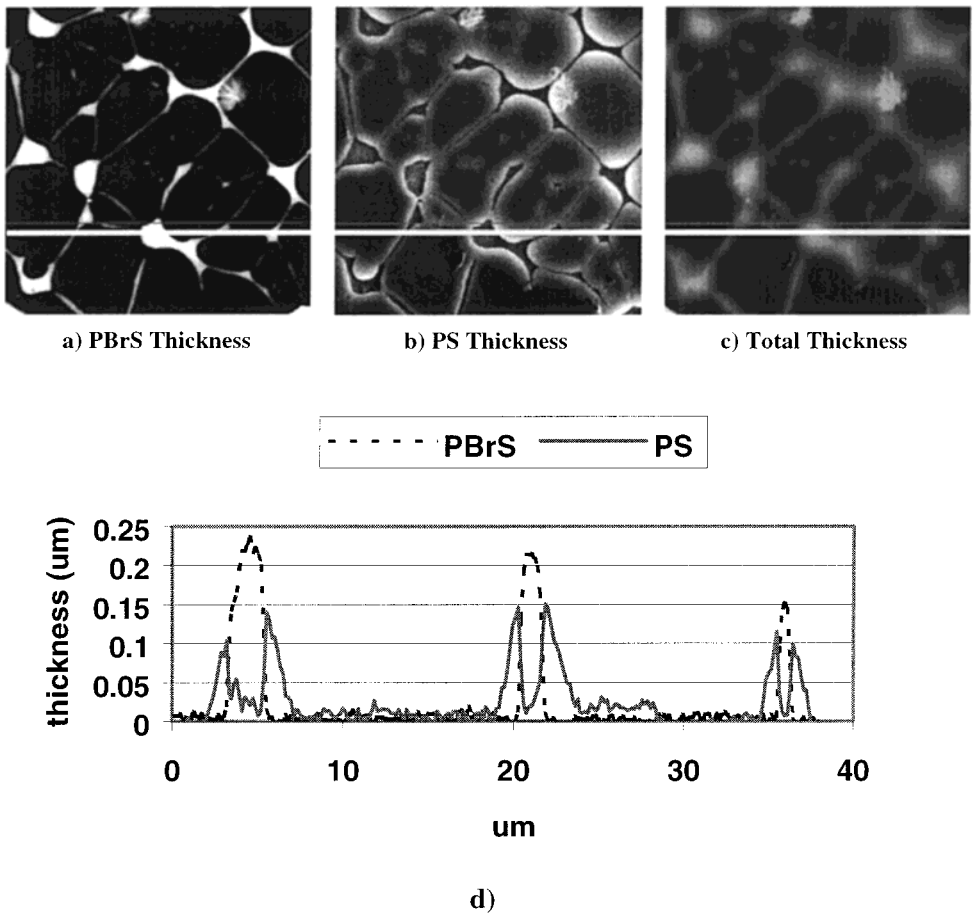


**Figure 8.** Component thickness maps of an annealed PBrS/PS bilayer with a 334 Å thick PS sublayer and 300 Å PBrS overlayer. Image area is 38 $\mu$m by 38 $\mu$m (240 × 240 pixels). (a) PBrS map, (b) PS map, (c) total thickness (sum of PS and PBrS maps), (d) profiles of the row indicated by line in parts a−c. Note: Lower display limit of images is set to black for zero thickness and upper limit is scaled for is maximum contrast.

will return to this issue below when we discuss the three-dimensional composition map of the droplets.

The STXM images of the PBrS, PS, and total polymer film thickness of a sample of a PS layer thickness of 334 Å are shown in Figure 8, where the brightness is proportional to the effective thickness. Figure 8a corresponds to the PBrS equivalent thickness map, while Figure 8b corresponds to the PS map. A total thickness map, obtained by summing the PS and PBrS images, is shown in Figure 8c. The profiles corresponding to the cross-section marked by the white lines in the three images are displayed in Figure 8d. From the figure, we can determine the actual percentage of the different polymers in the structures. From the STXM images (Figures 8a−d), it is clear that the $PBr_{x=0.79}S$ rich regions correspond to the raised sections seen in the AFM topographical scans. From the cross-sectional scans we can see that the PBrS regions are surrounded by raised PS regions encapsulating the PBrS at the edges. Since STXM data are acquired in transmission mode, the location of the PS detected in the regions of the PBrS is not uniquely determined in the direction normal to the surface; the PS could be above or below the PBrS. The location of the PS is obtained from PEEM, which is a surface sensitive technique.[22] PEEM images and local spectra show that, for thick PS sublayers, the PBrS domains are fully encapsulated; i.e., no PBrS peek is seen in the spectra. This is not surprising given the fact that the surface tension of PS is lower than that of PBrS. When the substrate layer thickness decreases, a PBrS peak is now observed in the NEXAFS data (Figure 9), indicating that the PBrS is no longer encapsulated. This is consistent with the model that when the PS layer becomes on the order of $R_g$, it is pinned to the Si and can no longer flow around the droplets to encapsulate them. STXM data show, (Figure 8) that partial encapsulation does occur along the sides of the droplets. In a previous paper,[23] it was shown that the dynamics of full encapsulation are much slower than those of the dewetting process, or the partial encapsulation shown in Figure 4.

It is possible to calculate the topographical contact angle ($\theta_A$) from the PS thickness STXM data by extrapolating a baseline from the points, as seen in Figure 10 which is from a section of Figure 8d. The areas with no PBrS are used as the baseline, and the increasing slopes of the area containing PBrS form the contact angle. We find that $\theta_A$ is in good quantitative agreement with the topographical AFM data that can also be seen in Figure 5. The large discrepancy between the calculated and observed angles can then be explained in terms of the encapsulating layer of PS at the droplet edge. As has been argued previously by authors in refs 24−26[24−26] for auto dewetting of a homopolymer on a brush, the stretching energy of the

(22) Tonner, B. P.; Dunham, D.; Droubay, T.; Kikuma, J.; Denlinger, J.; Rotenberg, E.; Warwick, A. *J. Electron Spectrosc. Relat. Phenom.* **1995**, *75*, 309.

(23) Ade, H.; Winesett, D. A.; Smith, A. P.; Anders, S.; Stammler, T.; Heske, C.; Slep, D.; Rafailovich, M. H.; Sokolov, J.; Stohr, J. *Appl. Phys. Lett.* **1998**, *73*, 25, 3775.

(24) Liebler, L.; Ajdari A.; Mourran, A. *Proceedings of the OUMS Conference*, Osaka, Japan, 1993.

(25) Liebler, L.; Mourran., A. *MRS Bull.* **1997**, *22*, 33.

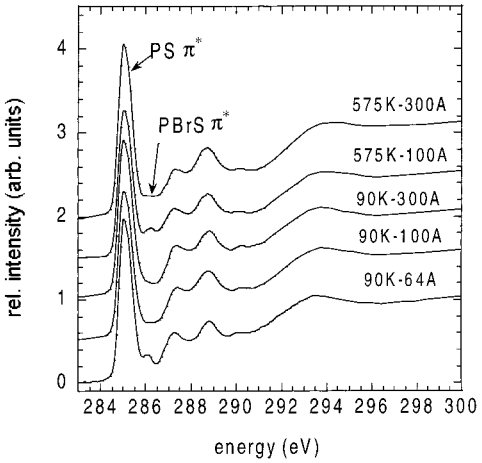


**Figure 9.** NEAXFS spectra of annealed bilayers in the final (equilibrium) state after 4 days of annealing at 180 °C. Indicated are the molecular weight and thickness of the lower PS layer. In all cases the top layer was 90K MW 300 Å PBrS. The PBrS $\pi$* reasonance is still clearly visible for the 90K MW/64 Å PS layer and 575K MW/100 Å PBrS layer, indicating that full encapsulation was not reached. For the 90K MW/100 Å and 90K MW/300 A the PBrS $\pi$* resonance is no longer visible indicating full encapsulation of the PBrS by PS.

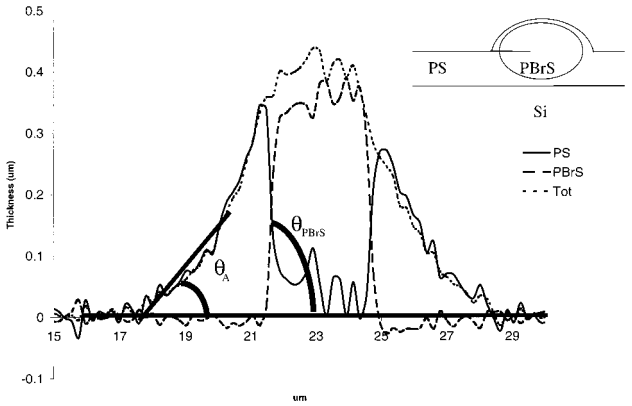


**Figure 10.** A blown up area of an STXM profile with a graphical depiction of the topographical contact angle ($\theta_A$) and the angle formed with PBrS and PS STXM data by extrapolating a base line from the points as seen in the figure. The areas with no PBrS are used as the base line, and the increasing slopes of the area containing PBrS form the contact angle. An embeded sketch representing the cross section of the scan.

polymer sublayer can be compensated for by increasing the interfacial area and decreasing the contact angle. The shape of the encapsulating layer at the droplet edge achieves the same purpose in this case. The contact angle for just the PBrS rich region with the PS layer inside the droplet ($\theta_{PBrS}$) can also be calculated from the STXM cross-section data of the PBrS scan, as seen in Figure 10. For a PS layer of 334 Å (Figure 5) it is found to be 27.4°. As discussed previously, the PS seen in the PBrS droplet in Figure 10 is not uniquely determined in the direction normal to the surface and encapsulation is determined by PEEM. From the theoretical model, eqs 7 and 9 imply a Neuman angle approaching 54°. The contact angle of the PBrS regions actually increases with PS thickness. This is because, unlike the thin rigid PS layer that forces the PBrS to act nearly as a liquid droplet on a solid substrate, the thicker PS layer approaches a liquid/liquid model as depicted in Figure 4. In the figure, interfacial forces are seen along with the proposed spring constant. The apparent contact angle is greater with a thick substrate layer, due to the change in shape of the PBrS droplet. For a thin PS layer, the model approaches a solid/liquid model except that there is PS forming a rim around the PBrS droplet as depicted in the figure. Hence, this shows how a full three-dimensional composition map can be used in order to extract information regarding the interface between homopolymers.

## 4. Conclusions

Complementary techniques were used to obtain three-dimensional concentration profiles of dewetted films of PBrS on the PS layer. The AFM results showed that the topographical contact angle at the polymer/air interface decreases exponentially with film thickness with a constant that is dependent upon the radius of gyration. The decay constant is approximately $3R_g$ for $M_w = 96K$ and $M_w = 575K$ polymers. The PEEM and STXM data show that the droplets consist of a PBrS core fully encapsulated by PS for substrates thicknesses greater than $R_g$. Only partial encapsulation is seen for substrates less than $R_g$. The Neuman angle, as determined from the PBrS STXM surface images, increases with substrate thickness. In contrast to simple liquids, we found that, for the case of entangled polymers, other factors such as the interfacial energy with the substrate, the film thickness, and the molecular weights must be considered. A model that includes a restoring force characterizing the change in elasticity of the substrate layer and the effects of an attractive surface provides good agreement with the experimental observations.

**Acknowledgment.** M.H.R. and J.S. are supported by National Science Foundation (NSF) Grant DMR-9732230 (MRSEC Program) and Department of Energy (DOE) Grant SG02-93-ER45481. H.A., D.A.W. and A.P.S. are supported by NSF Young Investigator Award DMR-9458060. STXM data acquired with the Stony Brook STXM at the NSLS developed by the group of Janos Kirz and Chris Jacobsen at SUNY Stony Brook, with support from the Office of Biological and Environmental Research, U.S. DOE under Contract DE-FG02-89ER60858, and NSF under Grant DBI-9605045. The zone plates were developed by Steve Spector and C. Jacobsen of Stony Brook and Don Tennant of Lucent Technologies Bell Labs, with support from the NSF under Grant ECS-9510499. The NSLS and ALS are supported by the Office of Basic Energy Sciences, Energy Research, Department of Energy.

LA990031B

(26) Liu, L.; Rafailovich, M. H.; Sokolov, J.; Zhong, X.; Eisenberg, A.; Kramer, E. J.; Sauer B. B.; Satija S. *Phys. Rev. Lett.* **1994**, *73*, 440.